Journal of Power Sources 195 (2010) 3047–3052

Contents lists available at ScienceDirect

Journal of Power Sources

journal homepage: www.elsevier.com/locate/jpowsour

Review

Preparation and electrochemical characterization of single-crystalline spherical $LiNi_{1/3}Co_{1/3}Mn_{1/3}O_2$ powders cathode material for Li-ion batteries

Xiaoyan Han, Qingfei Meng, Taolei Sun*, Jutang Sun*

Department of Chemistry, Wuhan University, Wuchang Luojiashan Road, Wuhan 430072, PR China

ARTICLE INFO

Article history:
Received 11 July 2009
Received in revised form 9 October 2009
Accepted 2 November 2009
Available online 24 November 2009

Keywords:
$LiNi_{1/3}Co_{1/3}Mn_{1/3}O_2$ single-crystalline sphere
Li-ion batteries
Cathode material
Electrochemical behavior
Rheological phase method

ABSTRACT

$LiNi_{1/3}Co_{1/3}Mn_{1/3}O_2$ has aroused much interest as a new generation of cathode material for Li-ion batteries, due to its great advantages in capacity, stability, low cost and low toxicity, *etc*. Here we report a novel single-crystalline spherical $LiNi_{1/3}Co_{1/3}Mn_{1/3}O_2$ material that is prepared by a convenient rheological phase reaction route. The X-ray powder diffraction, scanning electron microscopy and transmission electron microscopy indicate that the particles are highly dispersed with spherical morphologies and diameters of about 1–4 μm, and more interestingly, they show a perfect single-crystalline nature, which is not usual according to the crystal growth theories and may bring extra benefits to applications. Electrochemical tests show good performance of the material in both the capacity and cycling stability as cathode material in a model cell.

Contents

1. Introduction

Since $LiNi_{1/3}Co_{1/3}Mn_{1/3}O_2$ was reported for the first time by Ohzuku and Makimuar [1] in 2001, this material attracts great interest because of its great advantages over $LiCoO_2$, namely, higher capacity, milder structure and better stability, lower cost and less toxicity, *etc*. [2–4]. It has been considered to be one of the most promising cathode materials for Li-ion batteries that may replace the traditional material of $LiCoO_2$ [3–9]. Accordingly, considerable efforts have been performed to develop various $LiNi_{1/3}Co_{1/3}Mn_{1/3}O_2$ materials with different morphologies [10–19], while most of them are disordered agglomerations [14–19]. Among them, the spherical $LiNi_{1/3}Co_{1/3}Mn_{1/3}O_2$ materials are especially concerned due to the significant superiority in higher tap density and potentially higher thermal stability and safety, and have been realized by different methods. However, the resulting products are generally polycrystalline [20–29], and as far as we know, there is no report on the spherical single-crystalline $LiNi_{1/3}Co_{1/3}Mn_{1/3}O_2$ materials, due to the limitation of the conventional crystal growth mechanism in case of non-melt and/or without template.

On the other hand, the understanding of crystalline nature of a material is essential for the design and development of high-performance energy storage materials for Li-ion batteries. However, little attention has been paid on the crystalline nature of $LiNi_{1/3}Co_{1/3}Mn_{1/3}O_2$, materials [5,18] and the electrochemical properties of the single-crystalline $LiNi_{1/3}Co_{1/3}Mn_{1/3}O_2$

* Corresponding authors. Fax: +86 27 68754067 (PR China)/ 49 251 83 33602 (Germany).
E-mail addresses: sunt@uni-muenster.de (T. Sun), jtsun@whu.edu.cn (J. Sun).

0378-7753/$ – see front matter © 2009 Elsevier B.V. All rights reserved.
doi:10.1016/j.jpowsour.2009.11.007

micro-particles have never been evaluated, although it may bring some extra benefits to applications as cathode materials in Li-ion batteries. Here we report a novel spherical single-crystalline $LiNi_{1/3}Co_{1/3}Mn_{1/3}O_2$ material that is fabricated by a convenient rheological phase reaction route [30] using amorphous porous MnO_2 with micro-nano-structures as the raw material. The crystalline nature of this material and its electrochemical performance as cathode materials have been investigated.

2. Experimental section

2.1. Material preparation

Precursor $LiOH{\cdot}H_2O$, analytical reagent grade, was purchased from commercial sources. Precursor spherical amorphous MnO_2 (Fig. 1a) was prepared from potassium permanganate and manganese acetate, via a simple alternate drop-feeding process method. The alternate drop-feeding process is based on ethanol aqueous solutions (1:1) as matrix solutions. The potassium permanganate ($KMnO_4$, 0.25 mol L^{-1}, 200 mL) and manganese acetate ($MnC_4H_6O_4{\cdot}4H_2O$, 0.375 mol L^{-1}, 200 mL) aqueous solutions are dripped alternately into the ethanol aqueous solutions with stirring, then filtered, washed, and dried to yield amorphous MnO_2. The spherical NiO (Fig. 1b) was prepared by thermal decomposition of the grainy $NiC_2O_4{\cdot}2H_2O$ at 250 °C for 2 h, then 330 °C for 6 h in air. $(NH_4)_2C_2O_4{\cdot}H_2O$ (24.6 g) was added in nickel nitrate solution [$Ni(NO_3)_2{\cdot}6H_2O$ (50 g), H_2O (10 mL)] at 80–90 °C to form a rheological body with viscoelasticity. The ropy rheological body was fully dispersed with an appropriate amount of deionized water added, then filtered, washed, dehydrated with anhydrous ethanol and dried at 100 °C to get green $NiC_2O_4{\cdot}2H_2O$. The spherical Co_3O_4 (Fig. 1c) was prepared by thermal decomposition of the spherical $CoC_2O_4{\cdot}2H_2O$ at 250 °C for 8 h in air. $(NH_4)_2C_2O_4{\cdot}H_2O$ (12.8 g) was added in cobalt nitrate solution [$Co(NO_3)_2{\cdot}6H_2O$ (25 g), H_2O (15 mL)] at 80 °C to form a ropy rheological body. The ropy rheological body was dispersed with deionized water (48 g), then stirred for 1 h, deposited, filtrated, washed and dried at 120 °C to yield fuchsine $CoC_2O_4{\cdot}2H_2O$.

Preparation of single crystal $LiNi_{1/3}Co_{1/3}Mn_{1/3}O_2$ spherical powders was carried out using a rheological phase reaction route. $LiOH{\cdot}H_2O$ (purchased), MnO_2 (porous spherical, Self-prepared, Fig. 1a), NiO (spherical, Self-prepared, Fig. 1b) and Co_3O_4 (spherical, Self-prepared, Fig. 1c) were used as the starting materials in quantities corresponding to 0.12 mol stoichiometric $LiNi_{1/3}Co_{1/3}Mn_{1/3}O_2$ with a 5 mol% excess of Li. The chemicals were fully mixed by grinding and appropriate amount of water was added to get a rheological body. The mixture was transferred into a Teflon container and was then sealed in a stainless reactor at 80 °C for 5 h to give a grey precursor. After drying at 100 °C, the precursor was calcined at 420 °C for 1 h in air, taken out and ground, and then sintered at 950 °C for 10 h in air, resulting in black powders, single-crystalline spherical (denoted as SCS) sample. For comparison, another sample was also prepared from the commercial MnO_2 (Fig. 1d) of analytical reagent grade by the same procedure, which shows an irregular agglomeration nature (denoted as IA).

2.2. Measurements

The powder X-ray diffraction (XRD) patterns were obtained by a Shimadzu XRD-6000 diffractometer with a Ni filter and Cu $K\alpha_1$ radi-

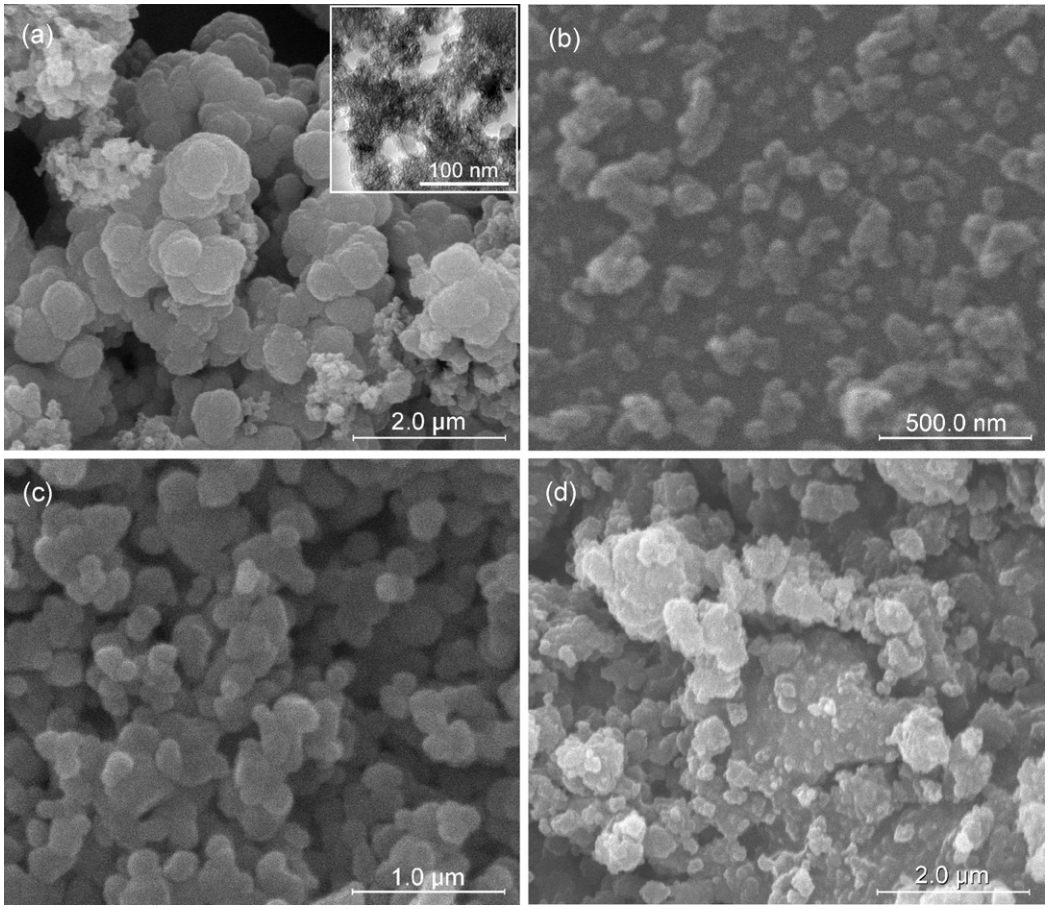

Fig. 1. SEM images for the starting materials that were used to prepare the $LiNi_{1/3}Co_{1/3}Mn_{1/3}O_2$ samples (SCS and IA). (a) Spherical porous MnO_2 particles. Inset is the typical TEM image, showing the porous structure of the particles. (b) Spherical NiO nano-particles. (c) Spherical Co_3O_4 nano-particles. (d) Commercial MnO_2 material.

ation (λ = 1.54056 Å), and the data were collected over 10–80° (2θ) with a scan speed of 4° min^{-1}. The refined crystal lattice parameters were calculated by the JADE5.EXE procedure. Chemical analysis was carried out by inductively coupled plasma atomic emission spectrometry (ICP-AES, IRIS Intrepid II XSP, Thermo Electron Corporation, USA). The particle size and morphology features were observed by scanning electron microscope (SEM, Hitachi X-650). The electron diffraction (ED) patterns were determined by means of transmission electron microscope (TEM, JEOL JEM-2010HT).

Electrochemical experiments were performed on a Neware cell test system at room temperature. The charge/discharge tests were carried out using the coin-type cell (size: 2016), which consisted of a working electrode and a lithium foil counter electrode separated by a Celgard 2300 microporous membrane. The working electrode was prepared by mixing the $LiNi_{1/3}Co_{1/3}Mn_{1/3}O_2$ powders, acetylene black and polytetrafluoroethylene (PTFE) binder, in the weight ratio of 80:15:5, and the mixture was then compressed onto a stainless steel mesh current collector. $LiPF_6$ solution (1 M) dissolved in EC/DMC (1:1 volume ratio) was used as the electrolyte. The cells were assembled in an argon-filled glovebox (Mikrouna, Super 1220/750). The cells were charged and discharged between 2.5 and 4.6 V vs. Li/Li$^+$ at a constant current density of 100 mA g^{-1}.

3. Results and discussion

The XRD pattern for the as-prepared SCS sample is shown in Fig. 2. All peaks can be indexed to the typical hexagonal α-$NaFeO_2$ type with $R\bar{3}m$ space group. Distinct splitting of (0 0 6)–(1 0 2) and (1 0 8)–(1 1 0) peaks can be observed, indicating that the sample possesses a well-developed layered-structure [4]. The hexagonal

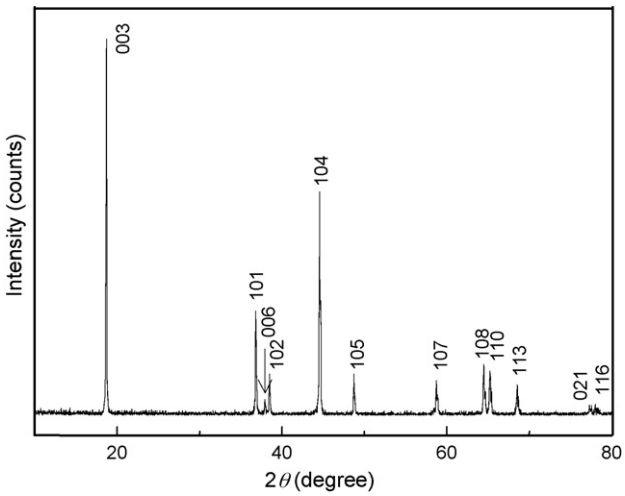

Fig. 2. Powder XRD pattern of $LiNi_{1/3}Co_{1/3}Mn_{1/3}O_2$ (SCS) prepared by a rheological phase reaction route.

lattice parameters a and c of the sample are determined to be 2.8636(2) and 14.2472(1) Å, respectively. These data agree well with those observed by Ohzuku and Makimura [1] (a = 2.867 Å and c = 14.246 Å) and Shaju et al. [3]. (a = 2.864 Å and c = 14.233 Å). The diffraction peaks are sharp and strong, and there are not other detectable peaks for impurity phases, indicating that the as-prepared $LiNi_{1/3}Co_{1/3}Mn_{1/3}O_2$ material is well crystallized and the product purity is very high. Chemical analysis confirmed the composition $Li_{0.99}(Ni_{0.34}Co_{0.33}Mn_{0.34})O_2$ within experimental error.

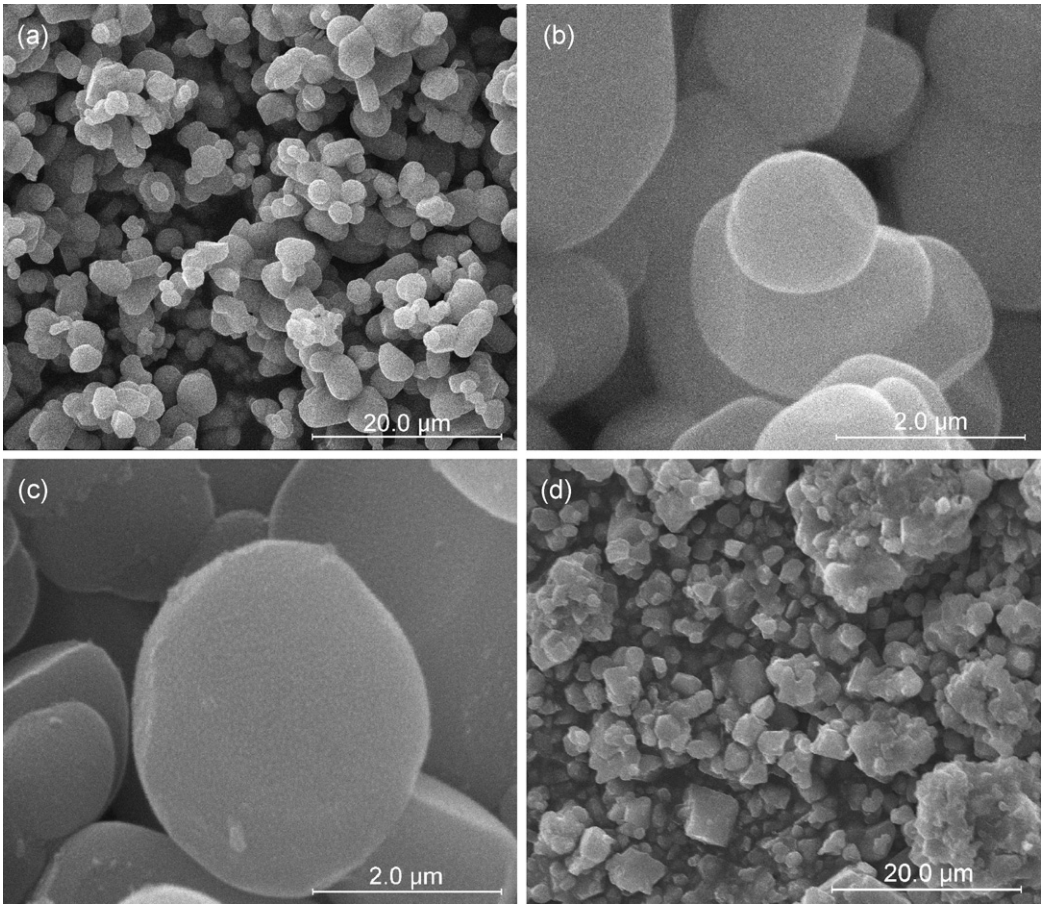

Fig. 3. SEM images of the as-prepared $LiNi_{1/3}Co_{1/3}Mn_{1/3}O_2$ ((a–c) SCS samples; (d) IA sample).

The Particle sizes and morphological features of $LiNi_{1/3}Co_{1/3}Mn_{1/3}O_2$ sample SCS were examined by SEM. As shown in Fig. 3a, the particles exhibit uniform spherical morphologies with diameters that mostly locate in the range of about 1–4 μm. The magnified SEM image (as typically shown in Fig. 3b) indicates that the surfaces of the particles are quite smooth and the particles are highly dispersed without agglomeration, which show a dense and homogeneous nature inside the particles, as revealed by the magnified image for a broken particle (Fig. 3c). In comparison, Fig. 3d is the SEM image of $LiNi_{1/3}Co_{1/3}Mn_{1/3}O_2$ sample IA prepared from commercial MnO_2, which shows irregular lump morphologies, and many fused together to form big agglomerates.

Fig. 4 shows the TEM images and electron diffraction patterns of two small $LiNi_{1/3}Co_{1/3}Mn_{1/3}O_2$ (SCS) spheres, the sizes of which are about 420 and 650 nm (it should be pointed out that, in order to make clear the single-crystalline nature of the $LiNi_{1/3}Co_{1/3}Mn_{1/3}O_2$ sphere, a full sphere should be located in the selected area of electron diffraction; therefore, small particles were selected here), respectively. In Fig. 4a, the interplanar distances (d) of diffraction spots are $d(a_1) = 2.3344$ Å, $d(a_2) = 1.4420$ Å and $d(a_3) = 1.2222$ Å, which could be indexed to the crystal planes (0 1 2), (1 0 $\bar{8}$) and (1 1 $\bar{6}$) in terms of $R\bar{3}m$ space group ($a = 2.8636$ Å, $c = 14.2472$ Å), respectively, and zone axis [8 $\bar{2}$ 1]. In Fig. 4b, the observed interplanar distances of diffraction spots are $d(b_1) = 2.3673$ Å, $d(b_2) = 2.3344$ Å and $d(b_3) = 1.4420$ Å, which were indexed to the crystal planes (0 0 6), (0 1 2) and (0 1 8), respectively, and zone axis [1 0 0]. It reveals that each $LiNi_{1/3}Co_{1/3}Mn_{1/3}O_2$ sphere of the SCS sample is a perfect single crystal.

Based on the above results, we proposed the growth mechanism of spherical $LiNi_{1/3}Co_{1/3}Mn_{1/3}O_2$ single crystals: The amorphous polyporous MnO_2 sphere with micro-nano-structure acts as the template for the crystal formation, and in the rheological phase reaction process, LiOH, nanoscale NiO and Co_3O_4 were inserted into the interspace and/or adsorbed on the surface of spherical MnO_2 to form new spherical composite oxide with nano-structure. The melting point of nano-structure composite oxide would be far lower than ordinary metal oxide, therefore, it will present glass-like melt at the high temperature of the calcination step, which may result in the spherical morphology due to the surface tension of the melt, and at the same time, single crystals grow through cationic diffusion reaction and ionic rearrangement.

The initial charge/discharge curves of two $LiNi_{1/3}Co_{1/3}Mn_{1/3}O_2$ electrodes between 2.5 and 4.6 V at a constant current density of 100 mA g^{-1} are shown in Fig. 5. It can be seen that the initial charge and discharge behaviors for SCS and IA are similar. They show charge capacities of 209 and 215 mAh g^{-1} and discharge capacities of 177 and 179 mAh g^{-1}, respectively. The initial coulomb efficiencies for SCS and IA are 85% and 83%, respectively. Sample SCS has a lower initial discharge capacity but higher initial coulomb efficiency than that of sample IA. Moreover, the spherical single-crystalline $LiNi_{1/3}Co_{1/3}Mn_{1/3}O_2$ (SCS) materials deliver much higher initial charge and discharge capacity than the previous reported spherical polycrystalline $LiNi_{1/3}Co_{1/3}Mn_{1/3}O_2$ materials [20–23].

Fig. 6 shows the voltage vs. specific capacity profiles of $LiNi_{1/3}Co_{1/3}Mn_{1/3}O_2$ electrode (sample SCS) for different cycles

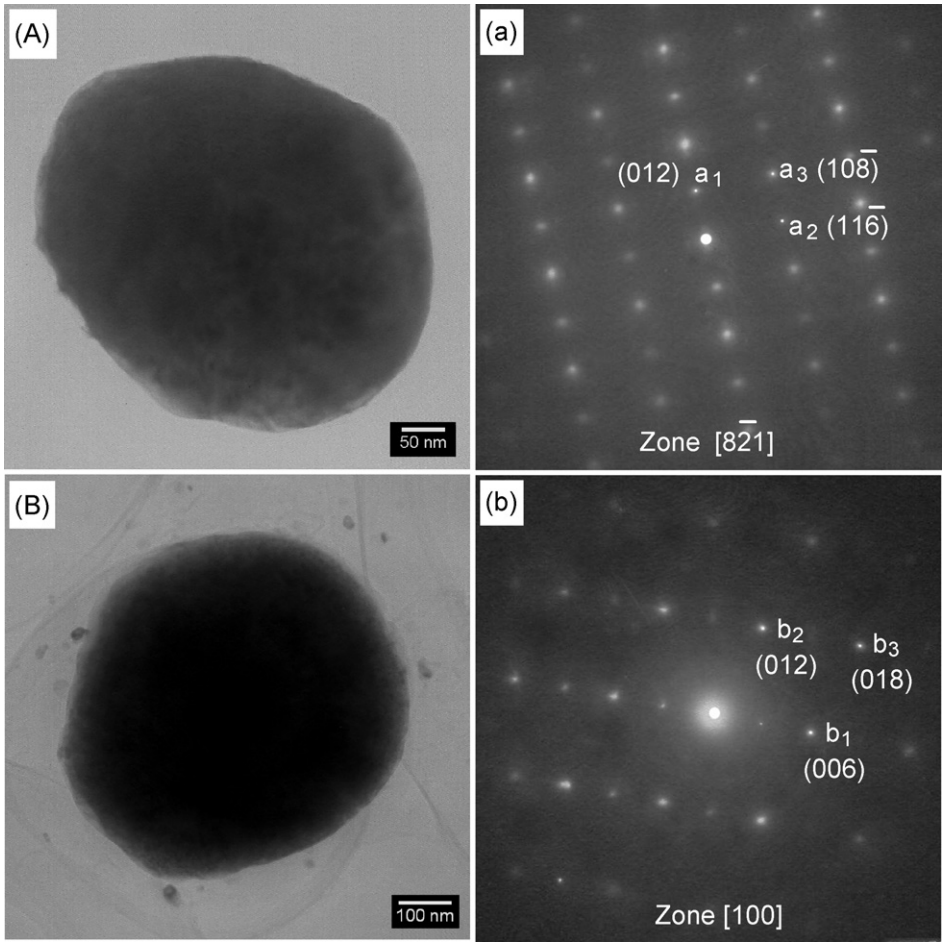

Fig. 4. TEM images (A, B) and electron diffraction patterns (a, b) of $LiNi_{1/3}Co_{1/3}Mn_{1/3}O_2$ single crystal spheres. The full sphere was located in the selected area of electron diffraction.

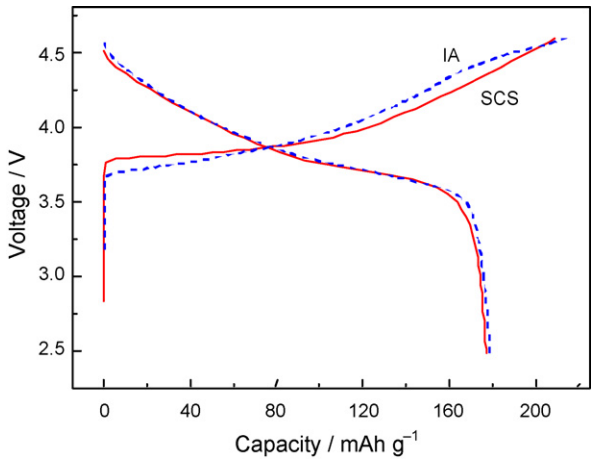

Fig. 5. The initial charge/discharge curves of $LiNi_{1/3}Co_{1/3}Mn_{1/3}O_2$ electrode (SCS sample and IA sample) between 2.5 and 4.6 V at a constant current density of 100 mA g^{-1}.

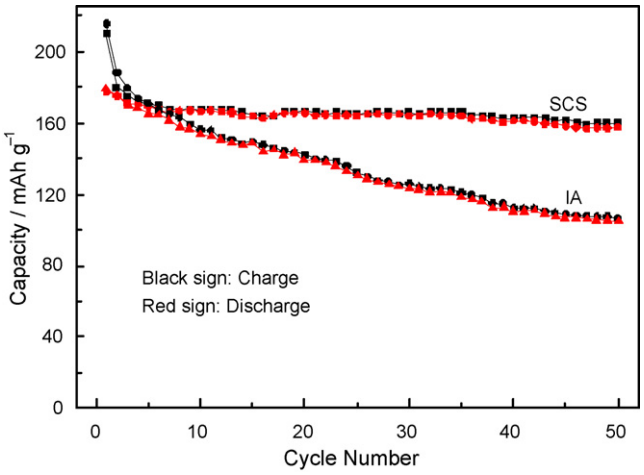

Fig. 7. Cyclic performance of $LiNi_{1/3}Co_{1/3}Mn_{1/3}O_2$ electrode (SCS sample and IA sample) between 2.5 and 4.6 V at a constant current density of 100 mA g^{-1}.

(1st, 2nd, 25th, 50th cycles), in which typical charge/discharge characteristics for the SCS material can be observed. During the charging process, the charge plateau started at about 3.75 V, and slowly increased to about 4.6 V. The electrode shows an initial discharge capacity of 177 mAh g^{-1} with an irreversible capacity loss of 32 mAh g^{-1} during the first cycle and 157 mAh g^{-1} was retained at the 50th cycle. The origin of the irreversible capacity is complicated, which mainly comes from the fact that a part of Ni^{3+} cannot be reduced to Ni^{2+} after the first cycle [31], and/or some other interface reactions, especially for some materials of small particle sizes.

The cycling capacity of as-prepared $LiNi_{1/3}Co_{1/3}Mn_{1/3}O_2$ (sample SCS and IA) is shown in Fig. 7. The sample SCS delivers an initial discharge capacity of 177 mAh g^{-1} and maintains good cycling behavior after 50 cycles (157 mAh g^{-1}), the capacity loss is about 11%. In comparison, the sample IA displays very bad cycling stability. The initial discharge capacity of sample IA is 179 mAh g^{-1} and the capacity reduces quickly to 109 mAh g^{-1} after 50 cycles, the capacity loss is about 39%. It clearly shows a much better electrochemical performance for the spherical single-crystalline $LiNi_{1/3}Co_{1/3}Mn_{1/3}O_2$ powders than that of IA sample. More interestingly, the cycling stability of as-prepared spherical single-crystalline $LiNi_{1/3}Co_{1/3}Mn_{1/3}O_2$ (SCS) powder materials is also much better than previous reported spherical polycrystalline $LiNi_{1/3}Co_{1/3}Mn_{1/3}O_2$ materials [20,23,24]. Based on above results and discussion, the as-prepared spherical single-crystalline $LiNi_{1/3}Co_{1/3}Mn_{1/3}O_2$ (SCS) materials deliver high initial capacity and excellent cycling stability, which is much better than irregular agglomeration body (IA) and spherical polycrystalline $LiNi_{1/3}Co_{1/3}Mn_{1/3}O_2$ materials. The improved electrochemical characteristics may be attributed to the compositional homogeneity and the higher structural stability of the spherical single crystals; and the high crystallinity of powders may be another important factor affecting the electrode capacity [13].

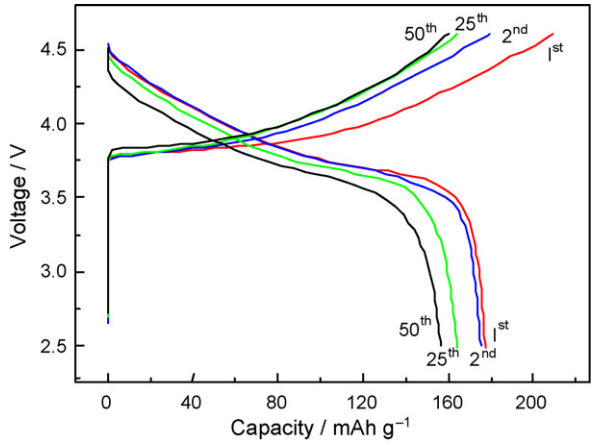

Fig. 6. Typical charge/discharge curves of $LiNi_{1/3}Co_{1/3}Mn_{1/3}O_2$ electrode (SCS sample) between 2.5 and 4.6 V at a constant current density of 100 mA g^{-1}.

4. Conclusions

In conclusion, a novel spherical $LiNi_{1/3}Co_{1/3}Mn_{1/3}O_2$ cathode material has been successfully prepared via a convenient rheological phase reaction route and precursors sintering method. The analysis of SEM, TEM images and XRD, ED patterns indicate that the particles of as-prepared $LiNi_{1/3}Co_{1/3}Mn_{1/3}O_2$ powders are solid spheres with clean and smooth surface, and each sphere is a perfect single crystal. The spherical $LiNi_{1/3}Co_{1/3}Mn_{1/3}O_2$ single crystal materials exhibit good electrochemical performance when being used as the cathode materials for Li-ion batteries. It shows that the spherical structure and the single-crystalline property may be important factors to improve the electrochemical performance of the material.

Acknowledgment

This work was supported by the National Natural Science Foundation of China (no. 20771087).

References

[1] T. Ohzuku, Y. Makimura, Chem. Lett. 30 (2001) 642–643.
[2] N. Yabuuchi, T. Ohzuku, J. Power Sources 119–121 (2003) 171–174.
[3] K.M. Shaju, G.V. Subba Rao, B.V.R. Chowdari, Electrochim. Acta 48 (2002) 145–151.
[4] B.J. Hwang, Y.W. Tsai, D. Carlier, G. Ceder, Chem. Mater. 15 (2003) 3676–3682.
[5] Y.W. Zeng, J. Power Sources 183 (2008) 316–324.
[6] W.S. Yoon, C.P. Grey, M. Balasubramanian, X.Q. Yang, D.A. Fischer, McBreen, Electrochem. Solid-State Lett. 7 (2004) A53–A55.
[7] T.H. Cho, S.M. Park, M. Yoshio, Chem. Lett. 33 (2004) 704–705.
[8] Y.M. Todorov, K. Numata, Electrochim. Acta 50 (2004) 495–499.
[9] J. Choi, A. Manthiram, J. Electrochem. Soc. 152 (2005) A1714–A1718.
[10] J.J. Liu, W.H. Qiu, L.Y. Yu, G.H. Zhang, H.L. Zhao, T. Li, J. Power Sources 174 (2007) 701–704.
[11] S. Patoux, M.M. Doeff, Electrochem. Commun. 6 (2004) 767–772.
[12] C.H. Lu, Y.K. Lin, J. Power Sources 189 (2009) 40–44.
[13] C.X. Ding, Q.S. Meng, L. Wang, C.H. Chen, Mater. Res. Bull. 44 (2009) 492–498.
[14] K.M. Shaju, P.G. Bruce, Adv. Mater. 18 (2006) 2330–2334.
[15] M.H. Lee, Y.J. Kang, S.T. Myung, Y.K. Sun, Electrochim. Acta 50 (2004) 939–948.

[16] S.H. Ju, H.Y. Koo, D.Y. Kim, S.K. Hong, Y.C. Kang, H.W. Ha, K. Kim, J. Mater Sci: Mater. Electron. 17 (2006) 353–359.
[17] M.V. Reddy, G.V. Subba Rao, B.V.R. Chowdari, J. Power Sources 159 (2006) 263.
[18] S.H. Park, C.S. Yoon, S.G. Kang, H.S. Kim, S.I. Moon, Y.K. Sun, Electrochim. Acta 49 (2004) 557–563.
[19] Y. Zhao, Y.Y. Wang, Q.Y. Lai, L.M. Chen, Y.J. Hao, X.Y. Ji, Synth. Metals 159 (2009) 331–337.
[20] Y. Kim, H.S. Kim, S.W. Martin, Electrochim. Acta 52 (2006) 1316–1322.
[21] J.G. Li, X.M. He, M.S. Fan, R.S. Zhao, C.Y. Jiang, C.R. Wan, Ionics 12 (2006) 77–80.
[22] X.J. Liu, G.Y. Zhu, K. Yang, J.Q. Wang, J. Power Sources 174 (2007) 1126–1130.
[23] H.C. Wu, Z.Z. Guo, M.H. Yang, C.H. Lu, T.Y. Wu, I. Taniguchi, Chem. Lett. 34 (2005) 1398–1399.
[24] S.K. Hu, G.H. Cheng, M.Y. Cheng, B.J. Hwang, R. Santhanam, J. Power Sources 188 (2009) 564–569.
[25] T.H. Cho, S.M. Park, M. Yoshio, T. Hirai, Y. Hideshima, J. Power Sources 142 (2005) 306–312.
[26] P. He, H.R. Wang, L. Qi, T. Osaka, J. Power Sources 160 (2006) 627–632.
[27] Z.X Tang, D.S. Gao, P. Chen, Z.H. Li, Q. Wu, Pure Appl. Chem. 80 (2008) 2537–2542.
[28] K. Amine, J. Liu, I. Belharouak, S.H. Kang, I. Bloom, D. Vissers, G. Henriksen, J. Power Sources 146 (2005) 111–115.
[29] Y.K. Sun, S.T. Myung, M.H. Kim, J. Prakash, K. Amine, J. Am. Chem. Soc. 127 (2005) 13411–13418.
[30] J.T. Sun, W. Xie, L.J. Yuan, K.L. Zhang, Q.Y. Wang, Mater. Sci. Eng. B 64 (1999) 157–160.
[31] Y.W. Tsai, B.J. Hwang, G. Ceder, H.S. Sheu, D.G. Liu, J.F. Lee, Chem. Mater. 17 (2005) 3191–3199.